A Sustainable Oxide Electrocatalyst for Hydrogen and Oxygen-Evolution Reactions

Ram Krishna Hona^{a,8,1}, Surendra B. Karki^{a,1}, Tengfei Cao^{b,1}, Rohan Mishra^b, George E. Sterbinsky^c, Farshid Ramezanipour^{a,*}

^aDepartment of Chemistry, University of Louisville, Louisville, Kentucky 40292, USA

[§]Current address: Department of Tribal Environmental Science, United Tribes Technical College, Bismarck, ND, USA

^bDepartment of Mechanical Engineering & Materials Science, and Institute of Materials Science & Engineering, Washington University in St. Louis, St. Louis, MO 63130, USA

^cX-ray Science Division, Advanced Photon Source, Argonne National Laboratory, Lemont, IL 60439, USA

*Corresponding author. Email: farshid.ramezanipour@louisville.edu, Phone: (502) 852-7061

Abstract

An electrocatalyst for water-splitting based on earth-abundant metals is reported. This perovskite-oxide catalyst, CaSrFe_{0.75}Co_{0.75}Mn_{0.5}O_{6- δ} (CSFCM), is examined using both experimental and computational methods. It demonstrates a combination of properties, which include (a) very high activity for oxygen-evolution reaction, with an overpotential of η = 0.19 V at 10 mA/cm², (b) high stability over 1000 cycles of catalysis, (c) the ability to catalyze hydrogen-evolution reaction effectively in both acidic and basic conditions, and (d) catalytic activity as a single-phase bulk material, without the need for any additional processing, multi-component composite preparation, or nanofabrication. Therefore, the catalytic activity of CSFCM is intrinsic, making it a good benchmark compound for future studies of electrocatalytic parameters. This work also highlights the impact of systematic structural design on electrocatalytic activity. Results from density-functional-theory calculations indicate that in addition to an optimal e_g occupancy of \sim 1, an additional descriptor, i.e., maximizing the number of free e_g carriers, correlates with the electrocatalytic activity.

Keywords: electrocatalyst, water-splitting, earth-abundant metals, perovskite-oxide, oxygen-evolution reaction, hydrogen-evolution reaction

¹These authors contributed equally to this work

1. Introduction

The discovery of efficient, stable and economical electrocatalysts for oxygen-evolution and hydrogen-evolution reactions is essential to water electrolysis. In addition to water splitting, the oxygen evolution reaction (OER)¹ is a key process in solar energy utilization,² rechargeable metalair batteries,³ and regenerative fuel cells.⁴ However, this reaction is a multistep four-electrontransfer process with high activation energy.⁵ The high cost of conventional OER catalysts, such as IrO₂ and RuO₂, has hindered their practical applications. As a result, much effort has been dedicated to the discovery of new catalysts based on earth-abundant metals that can compete with precious metal catalysts. In recent years, we have investigated multiple oxide materials for this purpose. 6-11 One promising family of materials for OER are oxygen-deficient perovskites, which show significant catalytic activity and stability. Their well-defined structure and compositional versatility make it possible to tune their electrocatalytic properties by modification of atomic composition. Their general formula is $ABO_{3-\delta}$, where large A cations reside in spaces between $BO_{6-\delta}$ polyhedra (Figure 1). In these materials some of the oxygen sites, that are occupied in a typical perovskite, are vacant. Several members of the oxygen-deficient perovskite family have demonstrated good OER activity, Sr₂Fe₂O_{6-δ}, studied by our group.⁶ Other examples include $SrNb_{0.1}Co_{0.7}Fe_{0.2}O_{3-\delta}$, ¹² (BSCF),¹ $SrCo_{0.9}Ti_{0.1}O_{3-\delta_1}^{13}$ $Ba_{0.5}Sr_{0.5}Co_{0.8}Fe_{0.2}O_{3-\delta}$ Pr_{0.5}Ba_{0.3}Ca_{0.2}CoO₃₋₈, ¹⁴ with BSCF being a paradigmatic example against which new perovskite catalysts are often benchmarked.

For hydrogen evolution reaction (HER), the best electrocatalyst is Pt/C, which suffers from a similar problem as the precious metal catalysts for OER, namely high cost and lack of economic efficiency. Therefore, a range of materials have been studied for HER catalysis, such as phosphides, ¹⁵ sulphides, ¹⁶⁻¹⁸ nitrides, ¹⁹ carbides, ¹⁹ and oxides. ²⁰ Despite the relative success of oxygen-deficient perovskites in OER catalysis, few members of this family have shown HER activity in alkaline conditions. ^{21, 22} In addition, perovskite-type oxides based on non-precious metals that show HER activity in acidic conditions are rare. One study that briefly examined Labased perovskites, reported extremely low activity in acidic condition. ²³

Importantly, catalysts based on earth-abundant metals that have twofold catalytic properties and can catalyze both half-reactions of water-splitting are uncommon, especially among perovskite-type oxides. However, there are multiple examples of such catalysts based on platinum-group metals, Ru, Ir or Rh.²⁴⁻²⁶ In addition, multicomponent composites^{26, 27} have been explored

as catalysts with twofold properties. Some single-phase catalysts with twofold properties have also been reported, but they often require nanofabrication.^{28, 29} Catalytic materials that can be used in bulk form as catalysts for both OER and HER are uncommon.

In the present study, we report an outstanding perovskite oxide, CaSrFe_{0.75}Co_{0.75}Mn_{0.5}O₆₋₈ (CSFCM), which is capable of catalyzing both half reactions of water splitting in bulk form without the need for composite preparation, nanofabrication or any other type of processing. In particular, it shows a remarkably low overpotential for OER and retains its performance even after 1000 cycles. Using density-functional-theory (DFT) calculations, we find that the experimentally observed OER activity correlates with the number of free e_g carriers, which could be used as a descriptor, in addition to the e_g orbital occupancy, to further tailor the performance of oxide perovskite electrocatalysts.

2. Methods

- **2.1. Synthesis and structural characterization.** Solid-state synthesis method was used to prepare all materials. The powders of the precursor compounds CaCO₃ (Alfa Aesar, 99.95%), SrCO₃ (Alfa Aesar, 99.95%), Fe₂O₃ (Alfa Aesar, 99.998%), Mn₂O₃ (Sigma Aldrich,99.99%) and Co₃O₄ (Alfa Aesar, 99.7%), were mixed in stoichiometric proportions and ground together using an agate mortar and pestle, then pressed into a pellet and calcined in air at 1000 °C for 24 h. The samples were then reground and sintered at 1200 °C for 24 h in the same environment, followed by slow cooling. The heating and cooling rates were 100 °C/h in all cases. The structures of the polycrystalline materials were determined by Rietveld analyses with powder X-ray diffraction using Cu Ka1 radiation ($\lambda = 1.54056$ Å). The GSAS software³⁰ and EXPEGUI interface³¹ were used for Rietveld refinements. The sample morphologies were examined using high resolution field-emission scanning electron microscopy (SEM). X-ray photoelectron spectroscopy (XPS) was performed at room temperature using Al Ka radiation (1486.7 eV).
- **2.2. X-ray absorption near-edge structure (XANES).** XANES spectra were collected at beamline 9-BM of the Advanced Photon Source at Argonne National Laboratory. CaSrFe_{1-x}Co_{1-x}Mn_{2x}O_{6- δ} powders with x = 0.2, 0.25, 0.3 were studied at the Co, Fe, and Mn *K*-edges. The energy of the X-rays was selected with a Si (111) double crystal monochromator, and the X-ray beam was focused to a spot of approximately 500 μ m in diameter using a Rh coated toroidal mirror. Higher energy harmonics were rejected using a Rh coated flat mirror. XANES spectra from multiple

reference materials were also collected, including powders of CoO, LaCoO₃, FeO, Fe₂O₃, SrFeO₃, MnO, Mn₂O₃, and MnO₂. The absorption was determined by measurement of the X-ray transmission through the powder, which was either spread in a thin uniform layer onto tape, of which multiples were stacked, or pressed into a pellet after dilution with polyethylene glycol powder. Details of the XANES data analysis and fitting methods are provided in the Supporting Information.

2.3. Electrode preparation and electrochemical measurements. Catalyst ink was prepared by sonicating a mixture of 35 mg perovskite powder, 40 μ L Nafion and 7 mL THF for 30 minutes. Then 40 μ L of the ink was drop-casted (four coatings of 10 μ L each) on the surface of a glassy carbon electrode (with area of 0.196 cm²) and allowed to air-dry overnight. Experiments were also done by addition of 7 mg carbon black to the above mixture. For CSFCM, the results without or with carbon black were similar.

Electrocatalytic OER experiments were done using a three-electrode setup. The glassy carbon electrode loaded with catalyst was used as the working electrode and was rotated using a rotating disk electrode system at 1600 rpm. A commercial Pt electrode and silver/silver chloride electrode were used as counter and reference electrodes, respectively. The OER cyclic voltammetry data were recorded at a scan rate of 10 mV s⁻¹ versus Ag/AgCl (3 M KCl), as commonly done for OER experiments. 12-14, 32 The potential range that was scanned in OER experiments was 0.0 to 0.8 V (vs Ag/AgCl) for basic and 0.0 to 2.1 V (vs Ag/AgCl) for acidic condition. The HER data were obtained using a carbon counter electrode at a scan rate of 10 mV s⁻¹ versus Ag/AgCl (4 M KCl), as commonly utilized in HER.³³⁻³⁵ The electrode preparation and data collection procedure were the same for measurements on all samples and reference materials. The potential range that was scanned in HER experiments was -0.5 to -1.6 V (vs Ag/AgCl) for basic and 0.0 to -1.0 V (vs Ag/AgCl) for acidic condition. The ohmic drop (iR) correction was made to all polarization curves by measuring solution resistance via AC impedance, which gave $31 - 50 \Omega$ for 0.1 M HClO₄, 50 $-63~\Omega$ for 0.1 M KOH, and 9 $-12~\Omega$ for 1 M KOH. The potential values versus silver/silver chloride ($E_{Ag/AgCl}$) were converted to be expressed against RHE according to the equation E_{RHE} = $E_{Ag/AgCl} + 0.059 \text{ pH} + E_{Ag/AgCl}^{0}$, where $E_{Ag/AgCl}^{0} = 0.21 \text{ V}$ for 3M KCl³² and 0.197 V for 4 M KCl.³⁶ Chronopotentiometry experiments were conducted to test the stability of the catalyst by applying the current of 10 mA and measuring the potential over time.

2.4. Density-functional-theory (DFT) calculations. DFT calculations, as implemented in the VASP package,³⁷ were used to investigate the electronic structure of CaSrFe_{0.8}Co_{0.8}Mn_{0.4}O₆, CaSrFe_{0.75}Co_{0.75}Mn_{0.5}O₆, and CaSrFe_{0.6}Co_{0.6}Mn_{0.8}O₆. To simulate the random distribution of the transition metal ions within small supercells for DFT calculations, we used special quasirandom structures (SQS) as implemented in the Alloy Theoretic Automated Toolkit (ATAT).^{38, 39} We adopted SQS supercells having paramagnetic order⁴⁰ with 100 atoms for CaSrFe_{0.75}Co_{0.75}Mn_{0.5}O₆ and CaSrFe_{0.8}Co_{0.8}Mn_{0.4}O₆, and 80 atoms for CaSrFe_{0.6}Co_{0.6}Mn_{0.8}O₆ (see Supplementary Information). PDOS of the compounds were calculated to analyze their electronic structure and orbital occupation. The effect of oxygen deficiency on the distribution and occupancy of the *eg* states in these compounds is simulated by introducing one oxygen vacancy within the supercells used above. The orbital hybridization between *eg* states of transition metal and 2*p* states of oxygen is calculated through integration of their shared area in the PDOS. Further information about DFT calculations is described in detail in the Supporting Information.

3. Results and Discussion

3.1. Crystal Structure

Initially, a series of oxygen-deficient perovskites with formula $CaSrFe_{1-x}Co_{1-x}Mn_{2x}O_{6-\delta}$ (x=0-1) were synthesized, as shown in Figure 1. The best electrocatalytic performance was observed in the composition $CaSrFe_{0.75}Co_{0.75}Mn_{0.5}O_{6-\delta}$ (CSFCM). The structural framework of this material is similar to that of a perovskite (Figure 1), but with partial occupancy on oxygen sites, as shown in Table S1. The oxygen-vacancies have a disordered distribution in the crystal lattice, which forms a cubic Pm-3m structure, as demonstrated by Rietveld refinement with X-ray diffraction data in Figure 1a. It is noted that the formation of the cubic structure is a function of the Mn stoichiometry. As shown in Figure 1b, the structure of materials in the series $CaSrFe_{1-x}Co_{1-x}Mn_{2x}O_{6-\delta}$ changes as the Mn concentration (represented by 2x) is increased systematically. The materials with 2x=0-0.2 form structures where the oxygen vacancies are ordered, leading to the so-called brownmillerite type structure (Figure 1b), in which the transition metals have alternating octahedral and tetrahedral coordination.⁴¹ The 2x=0.3 phase is an intermediate where the transformation of brownmillerite to cubic perovskite structure begins. The compound with 2x=0.4 shows cubic structure with relatively wide diffraction peaks, which indicate that transformation

to the cubic structure is incomplete. Finally, the compounds with 2x = 0.5 - 1.0 show cubic perovskite structure. We examined the electrocatalytic activity of the entire series, and among them, the compound with 2x = 0.5 showed the highest activity. Its superior performance compared with the adjacent compositions is shown in Figure S1. Therefore, this material, along with two adjacent compositions with 2x = 0.4 and 2x = 0.6, were studied in greater detail to develop the structure-property relationships. Scanning electron microscopy data (Figure S2) show similar average grain sizes for the three compounds. Oxygen vacancies have been found to influence the catalytic activity of perovskite-based catalysts. Ale-44 Therefore, iodometric titrations were carried out to determine the degree of oxygen-deficiency in CaSrFe_{0.75}Co_{0.75}Mn_{0.5}O_{6-\delta}. These titrations showed $\delta \approx 0.56$, for this compound, which indicates a significant degree of oxygen-deficiency. Clearly the presence of these oxygen-vacancies has an impact on the valence states of transition metals, which were studied by X-ray absorption spectroscopy, as described in the next section.

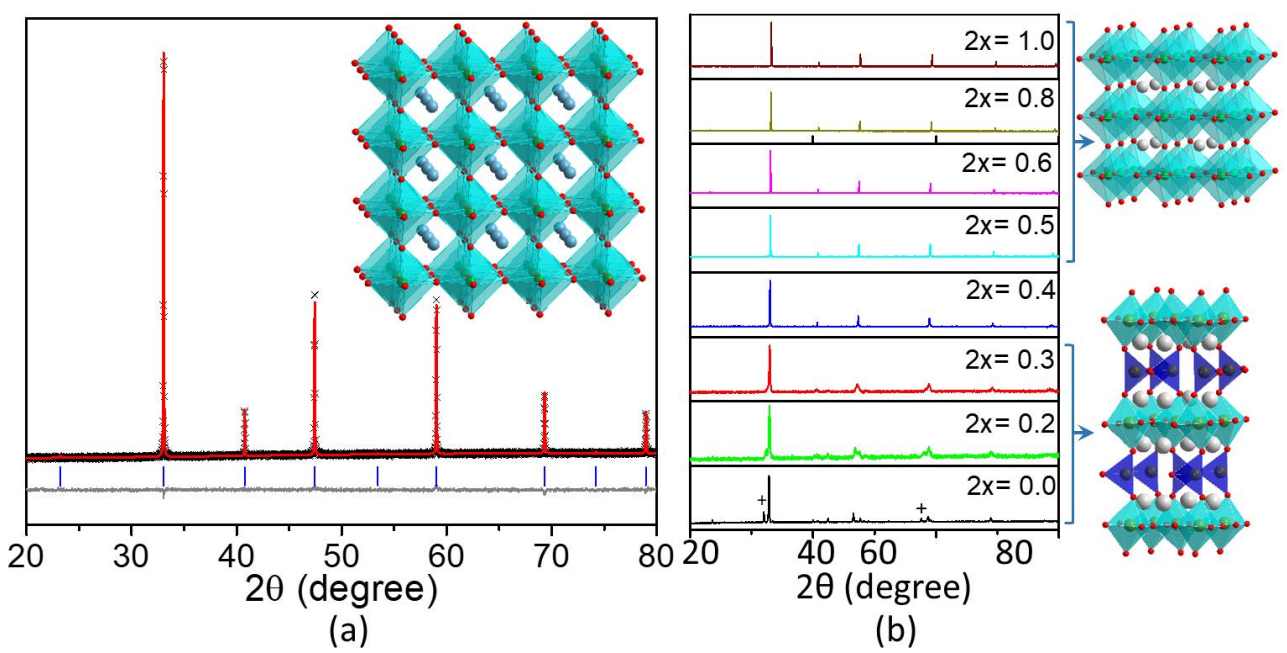


Fig. 1. (a) Rietveld refinement profile and crystal structure of CSFCM. (b) Change in the X-ray diffraction data for $CaSrFe_{1-x}Co_{1-x}Mn_{2x}O_{6-\delta}$ as a function of Mn-concentration, from brownmillerite structure (2x = 0 - 0.3) to perovskite structure (2x = 0.5 - 1.0). Crosses show two of the distinct brownmillerite peaks.

3.2. X-ray Absorption Near-Edge Structure

X-ray absorption near-edge structure (XANES), shown in Figure 2, was used for detailed analysis of the oxidation states of transition metals in CaSrFe_{0.75}Co_{0.75}Mn_{0.5}O_{6-δ} (CSFCM), as well as two adjacent compositions, containing 0.4 and 0.6 Mn per formula unit, i.e., CaSrFe_{0.8}Co_{0.8}Mn_{0.4}O_{6-δ} and CaSrFe_{0.7}Co_{0.7}Mn_{0.6}O_{6-δ}. In addition, XANES spectra were obtained on multiple reference materials, including powders of CoO, LaCoO₃, FeO, Fe₂O₃, SrFeO₃, MnO, Mn₂O₃, and MnO₂.

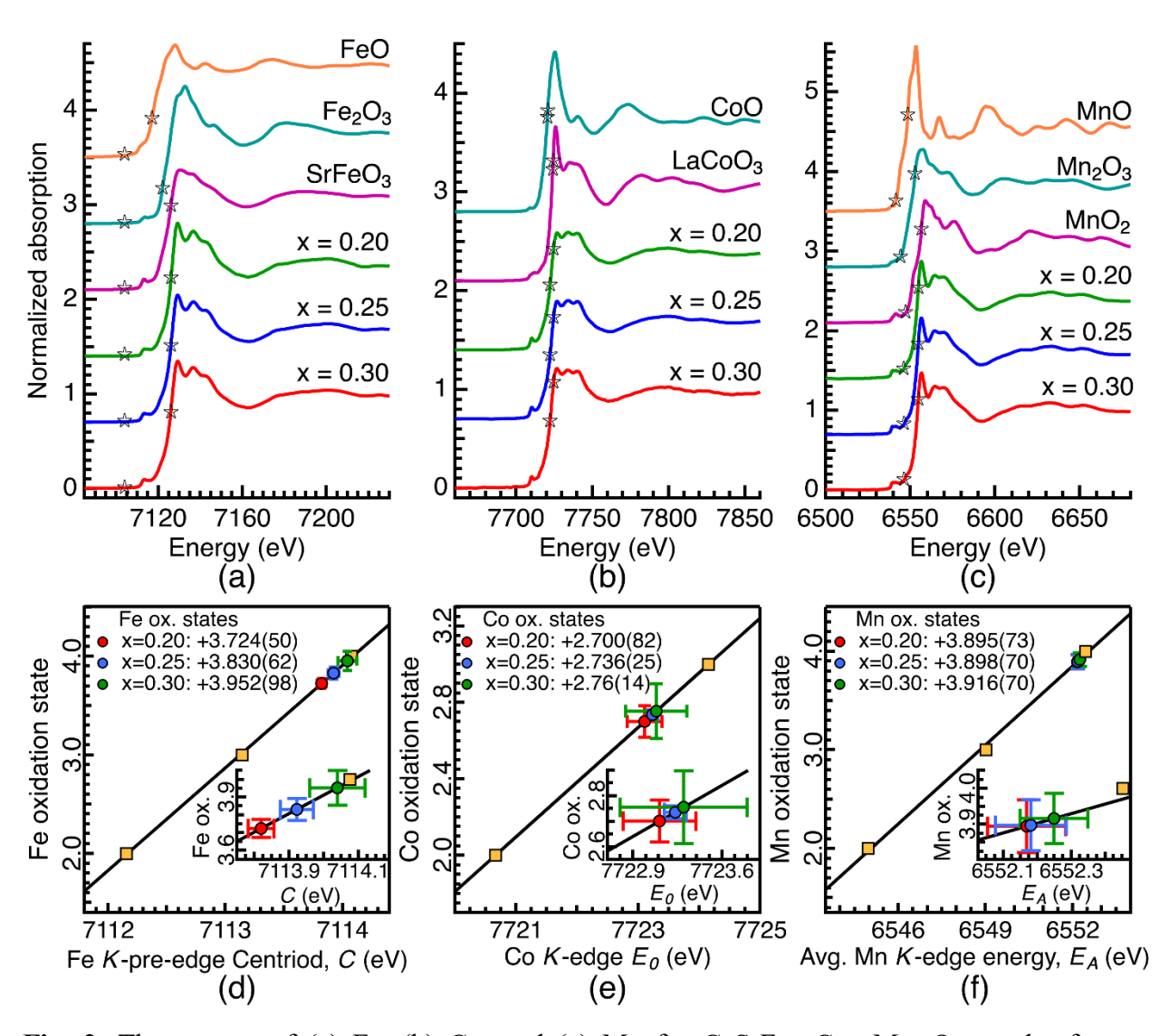


Fig. 2. The spectra of (a) Fe, (b) Co, and (c) Mn for CaSrFe_{1-x}Co_{1-x}Mn_{2x}O_{6-δ} and reference compounds. The edges used for determination of oxidation states are marked by asterisks. (d), (e) and (f) show the oxidation states of Fe, Co and Mn, respectively, in CaSrFe_{1-x}Co_{1-x}Mn_{2x}O_{6-δ} (x = 0.20, 0.25, 0.30) as well as in reference compounds FeO, Fe₂O₃, SrFeO₃, CoO, LaCoO₃, MnO, Mn₂O₃, and MnO₂. The straight line shows the fit.

Details of the XANES data analysis and fitting methods are provided in the Supporting Information. XANES experiments show that the Mn oxidation state is very similar in all three compounds, CaSrFe_{0.8}Co_{0.8}Mn_{0.4}O_{6-δ}, CaSrFe_{0.75}Co_{0.75}Mn_{0.5}O_{6-δ}, and CaSrFe_{0.7}Co_{0.7}Mn_{0.6}O_{6-δ}. As shown in Table S2, most of the manganese in these materials is in tetravalent state, with a smaller percentage of trivalent manganese. For iron, all three compounds contain a combination of trivalent and tetravalent states (Figure S3). However, there is a systematic increase in the iron oxidation state among these materials. A similar increase also appears to be present for the oxidation state of cobalt, although the variation is on the order of the measurement error. For all three compositions, the cobalt oxidation state is a combination of divalent and trivalent, as shown in Table S2.

3.3. Hydrogen and Oxygen-Evolution Activity

Since HER catalysts are commonly investigated in either alkaline, i.e., 1M KOH, ^{19, 34, 45} or acidic media, e.g., 0.1M HClO₄, ^{19, 45, 46} we examined CSFCM under both conditions. Although oxygen-deficient perovskites show good OER performance, very few compounds from this class of materials show catalytic activity for HER. The few examples that have been reported are HER-active in alkaline environment. ^{21, 22} Even less common are perovskite-type oxides based on non-precious metals that show HER activity in acidic media. A brief report on La-based perovskites shows very low HER activity in acidic conditions. ²³

Remarkably, CSFCM shows comparable HER activity in both acidic and basic conditions (Figure 3), a rare property for a perovskite-type oxide. The generally accepted mechanism for HER involves Volmer reaction, followed by either Heyrovsky or Tafel reaction, as shown below:^{45, 47}

Volmer reaction in acidic condition: $H_3O^+ + M + e^- \rightleftharpoons M - H^* + H_2O$

Volmer reaction in alkaline condition: $H_2O + M + e^- \rightleftharpoons M - H^* + OH^-$

Heyrovsky reaction in acidic condition: $M-H^* + H_3O^+ + e^- \rightleftharpoons M + H_2 + H_2O$

Heyrovsky reaction in alkaline condition: $M-H^* + H_2O + e^- \rightleftharpoons M + H_2 + OH^-$

Tafel reaction in both acidic and alkaline conditions: $2M-H^* \rightleftharpoons 2M + H_2$

The onset potential where the electrocatalytic activity commences and the polarization curve begins to depart from a flat line is one of the parameters used for comparing the activity of HER catalysts. Also, by convention, the overpotential required to achieve the current density of 10 mA/cm² (η_{10}) is taken as an indication of the performance of an electrocatalyst.^{48,49} CSFCM shows overpotentials of 0.35 V and 0.31 V in acidic and basic conditions, as shown in Figure 3. We note that CSFCM acts as a catalyst in bulk form with no additional processing. Also, as presented in Figure 3, it shows high stability over 12 hours.

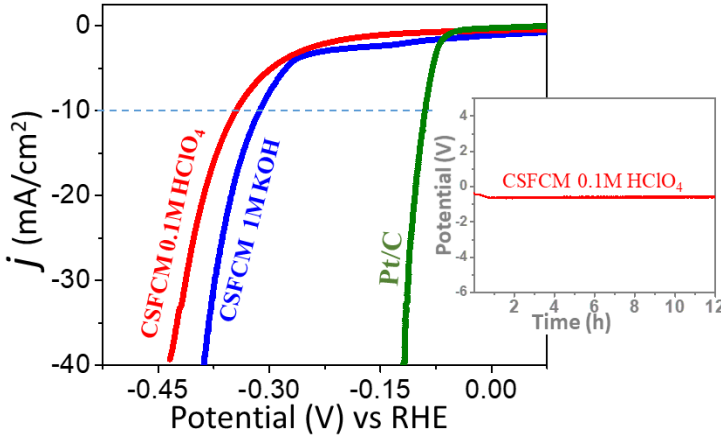


Fig. 3. HER polarization curves for CSFCM in acidic and basic conditions. The inset shows the stability over 12 hours in 0.1 M HClO₄.

The OER activity was also studied for CSFCM along with that of the precious metal catalyst RuO₂. Carbon black is generally added to the electrode composition during OER measurements to enhance the conductivity within the electrode and improve the utilization of the catalyst. ⁵⁰⁻⁵² However, recent studies have shown that the role of carbon is more complex than originally thought. ^{53, 54} For example, it has been shown that during the preparation of Ba_{0.5}Sr_{0.5}Co_{0.8}Fe_{0.2}O₃₋₈/carbon electrode, cobalt does not retain its valency and gets reduced. ⁵⁵ Therefore, OER experiments without carbon black are adopted by some researchers to avoid the interference from carbon. ⁵⁶ We performed OER experiments for the new compound, CSFCM, both without and with carbon black. Both methods gave similar results, indicating that the catalytic performance of this compound is not dependent on carbon black. The experiments without carbon are more desirable, as they demonstrate the intrinsic catalytic performance of the catalyst, without any contribution form carbon. Therefore, we used this method for further studies, where the

catalyst was dropcasted on the surface of a glassy carbon electrode without the addition of carbon black powder. The OER experiments are commonly done in 0.1 M KOH. We used the same condition to be able to directly compare our results to those reported for other catalysts. However, other conditions (1 M KOH and 0.1 M HClO₄) were also tested as shown in Figure S4. The best results were those of 0.1 M KOH, which is the typical OER condition. ^{1, 6, 12-14}

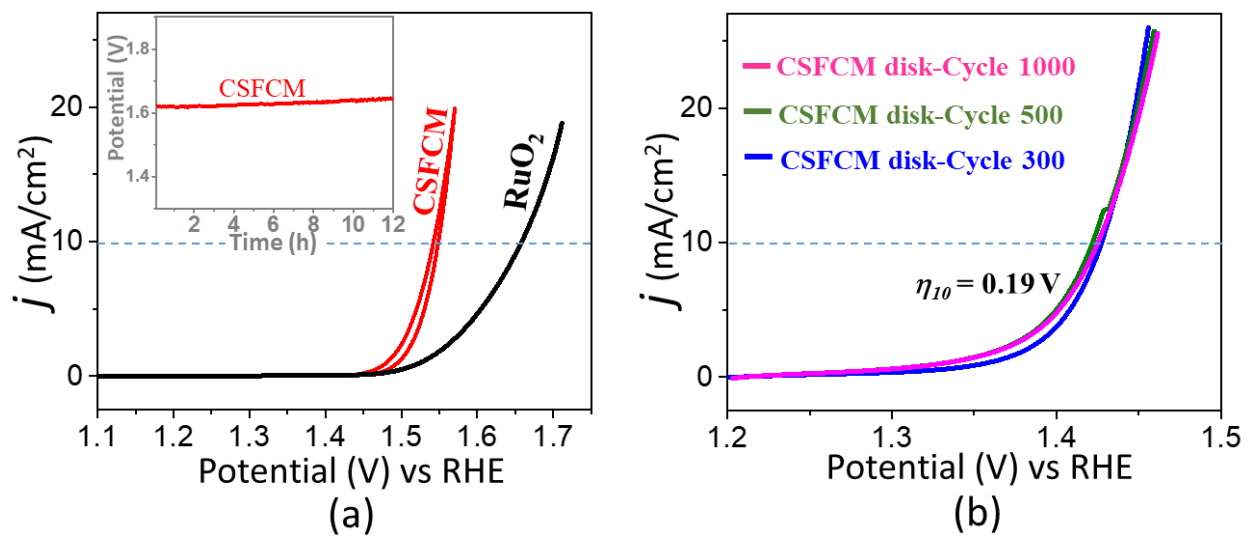


Fig. 4. (a) OER polarization curves in 0.1 M KOH for CSFCM and RuO₂ dropcasted on a glassy carbon electrode. The inset shows stability over 12 hours. (b) OER polarization curves for pure disk of CSFCM without glassy carbon electrode or any additives. Note the low overpotential, $\eta_{10} = 0.19 \text{ V}$, and excellent performance over 1000 cycles.

In addition, given the fundamental nature of this study, methods of investigation of the OER activity that can further examine the intrinsic catalytic properties by eliminating all other contributions, are highly desired. One of the electrode components that is nearly always used in OER studies is glassy carbon electrode, on which the catalyst is drop-casted. The glassy carbon electrode provides high electrical conductivity, while the catalyst film facilitates the OER. Recently some researchers have examined pure disks of catalytic materials to eliminate all electrode components, even the glassy carbon electrode. ^{57, 58} Given that the magnitude of OER potential is greater than that of HER, we speculated that the conductivity of the catalyst might be enough to be used alone without being loaded on a glassy carbon electrode. Therefore, in addition to the conventional glassy carbon method, we also conducted OER experiments using pure disks of the catalyst.

Again, the onset potential and the overpotential beyond the ideal potential of 1.23 V (at 10 mA/cm²) were evaluated. In 0.1 M KOH, the conventional drop-cast experiments for CSFCM give onset potential of 1.45 V and overpotential of $\eta_{10} \approx 0.31$ V (Figure 4a). The inset of Figure 4a shows the stability of this catalyst even after 12 hours. The pure disks of CSFCM show onset potential of 1.30 V and overpotential of $\eta_{10} \approx 0.19$ V (Figure 4b). In pure disk experiments, the whole surface of the disk contributes to the OER, leading to the enhanced overpotential. As shown in Figure 4b, the CSFCM disk shows excellent performance even up to 1000 cycles. In addition, CSFCM retains its structural integrity during the electrocatalysis process as evident form X-ray diffraction (Figure S5) and X-ray photoelectron spectroscopy data (Figure S6). The remarkable performance of CSFCM becomes more evident when its activity is compared to that of the traditional precious metal catalyst RuO₂, which shows overpotential of $\eta_{10} \approx 0.42 \text{ V.}^{59}$ Its activity is also superior to that of the highly regarded perovskite oxide BSCF, with overpotential of $\eta_{10} \approx$ 0.4 - 0.5 V. 12, 13, 60 While in recent years there have been reports of some catalysts with comparable OER overpotentials to CSFCM, they often utilize precious metals, either in the catalyst composition or as substrate. 61, 62 Such high OER activity in a non-precious-metal oxide is uncommon.

The kinetics of OER is commonly examined based on the Tafel equation η = a + b log j. ¹²⁻¹⁴ The slope of the Tafel plot, η vs. $\log j$, is indicative of the reaction rate. Smaller slope indicates smaller overpotential required to deliver the same current density increment, which implies faster electron-transfer and enhanced reaction kinetics. ⁴⁵ To obtain the Tafel slope, we first collected steady state chronoamperometry data (Figure S7) at different potentials starting from the OER onset potential. The steady state output currents from these measurements were then iR-corrected and plotted against the applied potentials. The overpotentials from these iR-corrected steady state data were then used to obtain the Tafel plots and Tafel slopes (Figure S7). As seen here, the Tafel slope for CSFCM is 71 mV/dec, as compared to ~71–94 mV/dc reported for the well-known BSCF catalyst. ^{12, 13, 60} This is consistent with the high OER activity of CSFCM and indicates the facile charge transport and enhanced kinetics. ⁶³

We also examined the electrochemically active surface area (ECSA) of CSFCM, as compared to RuO₂. This is often done using the electrochemical double layer capacitance (C_{dl}) of the catalysts using cyclic voltammetry in non-faradic region,⁶⁴ where electrode reactions are negligible and the electrical double layer charge and discharge is the main source of the current.⁶⁴,

 65 The ECSA value is related to C_{dl} through the relationship ECSA= $\!\!C_{dl}\!/C_{s}\!,$ where C_{s} is specific capacitance. ^{64, 66, 67} Irrespective of the C_s value, given the proportionality between the double layer capacitance, C_{dl}, and the electrochemically active surface area, ⁶⁸⁻⁷¹ it is common to take C_{dl} as a representative of the magnitude of ECSA. $^{69-71}$ The C_{dl} value is obtained using the equation C_{dl} = $\Delta j/v$, 69-71 where Δj is the absolute value of the difference between j_{anodic} and $j_{catodic}$ in cyclic voltammetry data and v is the scan rate. 69-71 Usually, Δi is plotted against v, and the value of C_{dl} is determined as half of the slope of this plot.⁶⁹⁻⁷¹ Alternatively, some researchers have used the plot of javerage versus v, where javerage is the average of the absolute values of janodic and jcatodic, ^{68, 72} and the slope is equivalent to C_{dl} without the need to divide by $2.^{68}$ Figure 5 shows the plot of Δi at the middle potential, 70 0.977 V, against the corresponding scan rates. The value of C_{dl} is determined by dividing the slope of this plot by 2.69-71 As shown in Figure 5, the C_{dl} for CSFCM is considerably larger than that of RuO₂, which is consistent with the high OER activity of CSFCM. Further analyses can also provide information about specific capacitance, as shown in Figure S8. In addition, the electrocatalytic activity can be normalized by C_{dl} instead of geometric surface area of the electrode. Figure S9 shows the C_{dl}-normalized activities of both CSFCM and RuO₂, which again indicates the significantly enhanced electrocatalytic performance of CSFCM compared to RuO₂.

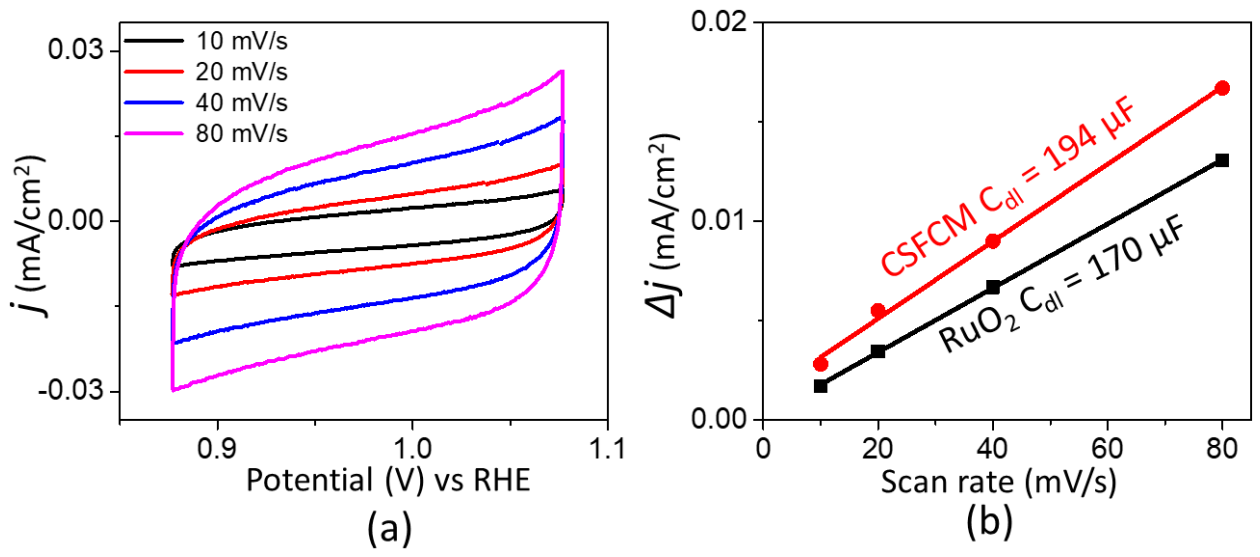


Fig. 5. (a) Cyclic voltammetry data in non-Faradic region with different scan rates for CSFCM. (b) The plot of Δj versus scan rate. The value of double layer capacitance, C_{dl} , is equivalent to half of the slope of this plot.

3.4. Electronic Structure

The electronic structure of perovskites, such as the filling of eg states of the transition metals, have been suggested to explain their catalytic activity. Initially, the high OER activity of BSCF led to the proposal that eg filling of near unity is optimum for obtaining the best OER performance.¹ Other researchers have since used this descriptor to explain the performance of various electrocatalysts for OER. $^{13, 73}$ The importance of e_g orbitals is that they form σ -bonding with oxygen-containing intermediates during the electrocatalytic process, unlike t_{2g} orbitals that form π -bonds. Therefore, the electron transfer between catalyst and reaction intermediates is more directly promoted by e_g orbitals.¹ Perovskite-related oxides with e_g electron occupation close to 1,1,22,73-75 have been reported to show high catalytic activity. This has been explained in terms of a moderate binding strength between the catalyst surface and reaction intermediates, optimizing both adsorption and desorption. It has been proposed that the catalyst-adsorbate interaction is relatively weak when e_g orbital occupation is larger than 1. Conversely, if e_g orbital occupation is less than 1, the strong bonding between the catalyst and the adsorbate can poison the catalyst by hindering the desorption process and reducing the number of available binding sites. A correlation between activity and $e_{\rm g}$ orbital filling has been suggested for some HER catalysts as well. ^{76,77} However, in many cases, the assignment of eg orbital occupancy has been done by electron count and based on the assumption of a certain spin state. 1, 13, 73, 76, 77

We used DFT calculations to investigate the electronic structure, and identify descriptors that lead to the enhanced electrocatalytic activity of CaSrFe_{0.75}Co_{0.75}Mn_{0.5}O_{6- δ} (CSFCM). We also calculated the electronic structure of two other compositions with lower and higher Fe/Co contents, namely CaSrFe_{0.6}Co_{0.6}Mn_{0.8}O_{6- δ} and CaSrFe_{0.8}Co_{0.8}Mn_{0.4}O_{6- δ}, to highlight the unique features of CSFCM. Initially, oxygen-vacancy-free models were examined and then vacancies were introduced into the structure. In both cases, the same trends for t_{2g} and e_g states were observed among the three materials. Figure 6 shows the projected density of states (PDOS) of t_{2g} and e_g states for the transition metals hybridized with the p states of oxygen. The 3d states of Fe and Co dominate the Fermi energy (E_F) with the empty e_g states of Mn being at relatively higher energies. Therefore, it is reasonable to assume that, in these CaSrFe_xCo_xMn_{2-x}O_{6- δ} catalysts, the Co and Fe sites determine the catalytic properties, as they can bind most easily with the adsorbates.

A quantitative analysis of the PDOS shows that $CaSrFe_{0.75}Co_{0.75}Mn_{0.5}O_6$, exhibits the highest density of e_g states (4.43×10⁻² states/eV) around E_F as shown in Table S3. We also find a

strong hybridization between e_g states of Co (1.37 e), Fe (1.41 e) and Mn (1.92 e) with oxygen 2p states in CaSrFe_{0.75}Co_{0.75}Mn_{0.5}O₆, which would suggest efficient charge transfer within the CaSrFe_{0.75}Co_{0.75}Mn_{0.5}O₆ structure. Stronger hybridization between the transition metal d states and oxygen p states is likely to facilitate efficient charge transfer between the transition metal and reaction intermediates during HER and OER.⁷⁸ The average hybridization of the three transition metals with O 2p is 1.57 e for CaSrFe_{0.75}Co_{0.75}Mn_{0.5}O₆, which is greater than that of CaSrFe_{0.6}Co_{0.6}Mn_{0.8}O₆ (1.25 e) and CaSrFe_{0.8}Co_{0.8}Mn_{0.4}O₆ (1.34 e). The PDOS of CaSrFe_{0.6}Co_{0.6}Mn_{0.8}O₆ and CaSrFe_{0.8}Co_{0.8}Mn_{0.4}O₆ are shown in Figure S11. Their e_g states around the Fermi energy are mainly comprised of Fe and Co contributions, similar to CaSrFe_{0.75}Co_{0.75}Mn_{0.5}O₆. However, the density of e_g states around the Fermi energy is reduced in these two compositions compared with CaSrFe_{0.75}Co_{0.75}Mn_{0.5}O₆, as shown in Table S3. Moreover, the average e_g states hybridization between different transition metals and oxygen 2p states in these two compounds is relatively small. Therefore, the catalyst-adsorbate charge transfer in CaSrFe_{0.6}Co_{0.6}Mn_{0.8}O₆ and CaSrFe_{0.8}Co_{0.8}Mn_{0.4}O₆ is expected to be weaker than that of CaSrFe_{0.75}Co_{0.75}Mn_{0.5}O₆, resulting in reduced catalytic activity.

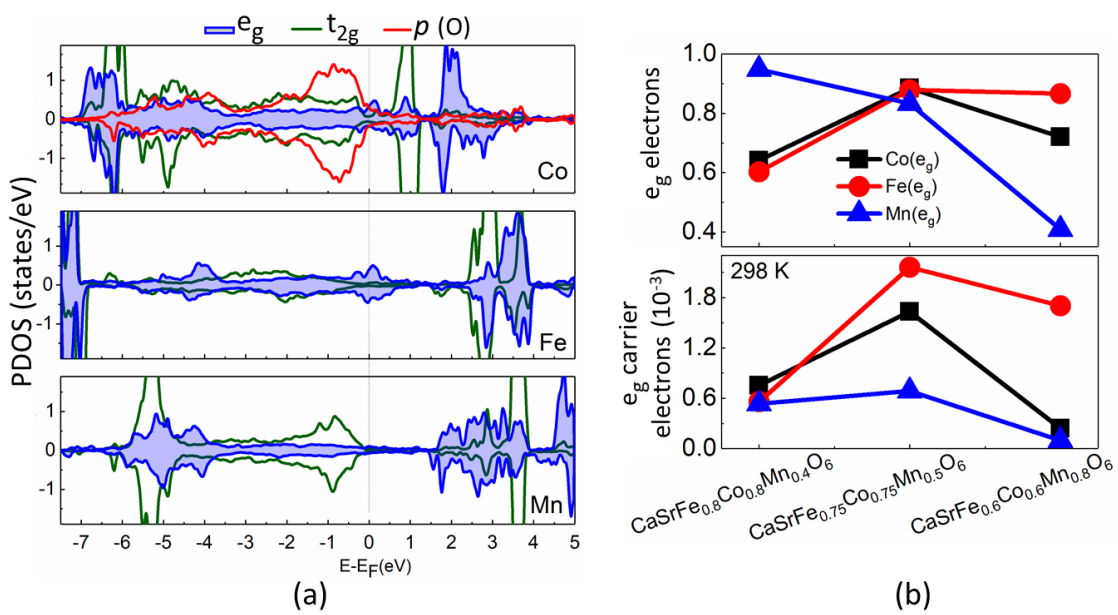


Fig. 6. (a) Spin-polarized projected density of states (PDOS) of e_g and t_{2g} state of Co, Fe and Mn, as well as oxygen 2p state for CaSrFe_{0.75}Co_{0.75}Mn_{0.5}O₆. (b) Top panel shows the average occupancy of e_g states of Co, Fe, Mn, and the bottom panel shows free e_g carriers at room temperature (298 K) in CaSrFe_{0.75}Co_{0.75}Mn_{0.5}O₆, CaSrFe_{0.8}Co_{0.8}Mn_{0.4}O₆, and CaSrFe_{0.6}Co_{0.6}Mn_{0.8}O₆.

We have calculated the e_g orbital occupation in CaSrFe_{0.75}Co_{0.75}Mn_{0.5}O₆, as well as CaSrFe_{0.6}Co_{0.6}Mn_{0.8}O₆ and CaSrFe_{0.8}Co_{0.8}Mn_{0.4}O₆, from the PDOS, shown in Figure 6 and Table S4. The results show that e_g orbital occupancy of the three transition metals in CaSrFe_{0.75}Co_{0.75}Mn_{0.5}O₆, is similar, with an average value of ~0.87e. The average e_g occupancy of the three transition metals decreases to 0.73e in CaSrFe_{0.8}Co_{0.8}Mn_{0.4}O₆ and 0.69e in CaSrFe_{0.6}Co_{0.6}Mn_{0.8}O₆. The relation between the e_g orbital occupancy and electrocatalytic activity has been previously studied for some other perovskite-type oxides, such as (Ln_{0.5}Ba_{0.5})CoO₃₋₈⁷³ and Nd_{1-x}Ba_xMnO₃₋₈.²² A similar effect has also been investigated for oxides such IrO₂, where Cu coping has been used to tune the electron occupation between t_{2g} and e_g states, resulting in the enhancement of electrocatalytic properties.⁷⁹

In addition to the e_g -occupancy, we find that the free e_g carriers can also be used as a descriptor for electrocatalytic activity in this class of compounds. An analysis of free e_g carriers at room temperature (Figure 6b) shows that the best catalyst, CaSrFe_{0.75}Co_{0.75}Mn_{0.5}O₆, has the largest free carriers among the three compounds. This indicates a more facile charge transfer between the catalyst and the reaction intermediates, which can enhance the catalytic activity.

It is noted that there is oxygen deficiency in all experimental samples, with the oxygen site occupancy being close to 0.90 for all materials. Therefore, we incorporated oxygen vacancies in DFT models (Figure S12) and analyzed the electronic structure of these compounds. The results show the same trend of e_g orbital distribution and occupation (Table S4) for the three compounds. The density of e_g states around E_F in CaSrFe_{0.75}Co_{0.75}Mn_{0.5}O_{6- δ} is again the largest among all compounds, and its average e_g orbital occupancy is higher than CaSrFe_{0.6}Co_{0.6}Mn_{0.8}O_{6- δ} and CaSrFe_{0.8}Co_{0.8}Mn_{0.4}O_{6- δ}.

Overall, DFT calculations show that the enhanced electrocatalytic activity of $CaSrFe_{0.75}Co_{0.75}Mn_{0.5}O_{6-\delta}$ can be attributed to: (a) greater density of e_g states around the Fermi energy, (b) optimum electron occupancy of e_g states, resulting in moderate binding between catalyst and reaction intermediates, (c) enhanced hybridization between transition metals and oxygen 2p states, and (d) the number of free e_g carriers, which in concert with optimum e_g -occupancy and hybridization, can facilitate efficient charge-transfer and enhance the electrocatalytic activity.

We note that electronic structure of these materials is a function of crystal structure and the ratio of transition metals, Fe/Co/Mn. While the optimum e_g filling correlates with high electrocatalytic activity, the underlying factors that lead to a certain type of e_g filling are indeed related to the structure and composition.

Conclusions

Controlled manipulation of the composition and structure can be a powerful tool in designing inexpensive electrocatalysts for water splitting based on transition metal oxides. Systematic control of the composition can result in structural transformations, which in turn affect the catalytic activity. We have shown that it is possible to find an optimum oxide system, with perovskite-type structure, which exhibits remarkable electrocatalytic properties for water splitting. The new catalyst, CSFCM, shows intrinsic catalytic activity in bulk form without the need for additional processing or microfabrication. This catalyst is highly stable and can be used for hundreds of cycles of catalysis. It features optimum e_g occupancy and free e_g carriers, which correlate with its high electrocatalytic activity.

Supporting Information

Detailed information about XANES analyses and DFT methods; tables of atomic positions, transition metal oxidation states from XANES, average e_g density of states around Fermi level, and e_g orbital occupations from DFT calculations; OER data for compounds with lower and higher Mn contents; SEM images, Fe K-edge XANES pre-edge data; OER data in different electrolytes; X-ray diffraction and XPS data before and after OER and HER; steady state chronoamperometry and Tafel plots; additional CVs for RuO₂ and CSFCM; C_{dl}-normalized OER data; charge transfer resistance under OER condition; additional spin-polarized projected density of states plots; atomic models used for DFT simulations.

Acknowledgements

This work is supported in part by the National Science Foundation (NSF) under grant no. DMR-1943085. The work at Washington University was supported by NSF DMREF grant no. CBET-1729787. This work used computational resources of the Extreme Science and Engineering Discovery Environment (XSEDE), which is supported by NSF grant number ACI-1548562. This

research used resources of the Advanced Photon Source, a U.S. Department of Energy (DOE) Office of Science User Facility operated for the DOE Office of Science by Argonne National Laboratory under Contract No. DE-AC02-06CH11357. GES thanks Mahalingam Balasubramanian, Steve M. Heald, and Chengjun Sun for helpful discussions regarding XANES analysis.

References

- 1. Suntivich, J.; May, K. J.; Gasteiger, H. A.; Goodenough, J. B.; Shao-Horn, Y., A Perovskite Oxide Optimized for Oxygen Evolution Catalysis from Molecular Orbital Principles. *Science* **2011**, *334*, 1383-1385.
- 2. Gray, H. B., Powering the Planet with Solar Fuel. *Nat. Chem.* **2009**, *1*, 7.
- 3. Lu, Y. C.; Xu, Z.; Gasteiger, H. A.; Chen, S.; Hamad-Schifferli, K.; Shao-Horn, Y., Platinum-Gold Nanoparticles: a Highly Active Bifunctional Electrocatalyst for Rechargeable Lithium-Air Batteries. *J. Am. Chem. Soc.* **2010**, *132*, 12170-12171.
- 4. Kumar, A.; Leonard, D.; Jesse, S.; Ciucci, F.; Eliseev, E. A.; Morozovska, A. N.; Biegalski, M. D.; Christen, H. M.; Tselev, A.; Mutoro, E.; Crumlin, E. J.; Morgan, D.; Shao-Horn, Y.; Borisevich, A.; Kalinin, S. V., Spatially Resolved Mapping of Oxygen Reduction/Evolution Reaction on Solid-Oxide Fuel Cell Cathodes with sub-10 nm Resolution. *ACS Nano* **2013**, *7*, 3808-3814.
- 5. Koper, M. T. M., Thermodynamic Theory of Multi-Electron Transfer Reactions: Implications for Electrocatalysis. *J.Electroanal. Chem.* **2011**, *660*, 254-260.
- 6. Hona, R. K.; Ramezanipour, F., Remarkable Oxygen-Evolution Activity of a Perovskite Oxide from the $Ca_{2-x}Sr_xFe_2O_{6-\delta}$ Series. *Angew. Chem. Int. Ed.* **2019**, *58*, 2060-2063.
- 7. Hona, R. K.; Ramezanipour, F., Effect of the Oxygen Vacancies and Structural Order on the Oxygen Evolution Activity: A Case Study of SrMnO_{3- δ} Featuring Four Different Structure Types. *Inorg. Chem.* **2020**, *59*, 4685-4692.
- 8. Karki, S. B.; Ramezanipour, F., Pseudocapacitive Energy Storage and Electrocatalytic Hydrogen-Evolution Activity of Defect-Ordered Perovskites $Sr_xCa_{3-x}GaMn_2O_8$ (x = 0 and 1). *ACS Appl. Energy Mater.* **2020,** *3*, 10983–10992.
- 9. Hona, R. K.; Karki, S. B.; Ramezanipour, F., Oxide Electrocatalysts Based on Earth-Abundant Metals for Both Hydrogen- and Oxygen-Evolution Reactions. *ACS Sustainable Chem. Eng.* **2020**, *8*, 11549-11557.
- 10. Alom, M. S.; Ramezanipour, F., Layered Oxides $SrLaFe_{1-x}Co_xO_{4-\delta}$ (x=0-1) as Bifunctional Electrocatalysts for Water-Splitting. *ChemCatChem* **2021**, 13, 3510-3516.
- 11. Hona, R. K.; Ramezanipour, F., Structure-Dependence of Electrical Conductivity and Electrocatalytic Properties of Sr₂Mn₂O₆ and CaSrMn₂O₆. *J. Chem. Sci.* **2019**, *131*, 109.
- 12. Zhu, Y.; Zhou, W.; Chen, Z. G.; Chen, Y.; Su, C.; Tadé, M. O.; Shao, Z., $SrNb_{0.1}Co_{0.7}Fe_{0.2}O_{3-\delta}$ Perovskite as a Next-Generation Electrocatalyst for Oxygen Evolution in Alkaline Solution. *Angew. Chem. Int. Ed.* **2015**, *54*, 3897-3901.
- 13. Su, C.; Wang, W.; Chen, Y.; Yang, G.; Xu, X.; Tadé, M. O.; Shao, Z., SrCo_{0.9}Ti_{0.1}O_{3-δ} as a New Electrocatalyst for the Oxygen Evolution Reaction in Alkaline Electrolyte with Stable Performance. *ACS Appl. Mater. Interfaces* **2015**, *7*, 17663-17670.
- 14. He, D.; He, G.; Jiang, H.; Chen, Z.; Huang, M., Enhanced Durability and Activity of the Perovskite Electrocatalyst $Pr_{0.5}Ba_{0.5}CoO_{3-\delta}$ by Ca Doping for the Oxygen Evolution Reaction at Room Temperature. *Chem. Commun.* **2017**, *53*, 5132-5135.

- 15. Yang, F.; Kang, N.; Yan, J.; Wang, X.; He, J.; Huo, S.; Song, L., Hydrogen Evolution Reaction Property of Molybdenum Disulfide/Nickel Phosphide Hybrids in Alkaline Solution. *Metals* **2018**, *8*, 359.
- 16. Benson, J.; Li, M.; Wang, S.; Wang, P.; Papakonstantinou, P., Electrocatalytic Hydrogen Evolution Reaction on Edges of a Few Layer Molybdenum Disulfide Nanodots. *ACS Appl. Mater. Interfaces* **2015**, *7*, 14113-14122.
- 17. Majidi, L.; Yasaei, P.; Warburton, R. E.; Fuladi, S.; Cavin, J.; Hu, X.; Hemmat, Z.; Cho, S. B.; Abbasi, P.; Vörös, M.; Cheng, L.; Sayahpour, B.; Bolotin, I. L.; Zapol, P.; Greeley, J.; Klie, R. F.; Mishra, R.; Khalili-Araghi, F.; Curtiss, L. A.; Salehi-Khojin, A., New Class of Electrocatalysts Based on 2D Transition Metal Dichalcogenides in Ionic Liquid. *Adv. Mater.* **2019**, *31*, 1804453.
- 18. Hemmat, Z.; Cavin, J.; Ahmadiparidari, A.; Ruckel, A.; Rastegar, S.; Misal, S. N.; Majidi, L.; Kumar, K.; Wang, S.; Guo, J.; Dawood, R.; Lagunas, F.; Parajuli, P.; Ngo, A. T.; Curtiss, L. A.; Cho, S. B.; Cabana, J.; Klie, R. F.; Mishra, R.; Salehi-Khojin, A., Quasi-Binary Transition Metal Dichalcogenide Alloys: Thermodynamic Stability Prediction, Scalable Synthesis, and Application. *Adv. Mater.* **2020**, *32*, 1907041.
- 19. Ma, L.; Ting, L. R. L.; Molinari, V.; Giordano, C.; Yeo, B. S., Efficient Hydrogen Evolution Reaction Catalyzed by Molybdenum Carbide and Molybdenum Nitride Nanocatalysts Synthesized via the Urea Glass Route. *J. Mater. Chem. A* **2015**, *3*, 8361-8368.
- 20. Nayak, A. K.; Verma, M.; Sohn, Y.; Deshpande, P. A.; Pradhan, D., Highly Active Tungsten Oxide Nanoplate Electrocatalysts for the Hydrogen Evolution Reaction in Acidic and Near Neutral Electrolytes. **2017**, *2*, 7039-7047.
- 21. Xu, X.; Chen, Y.; Zhou, W.; Zhu, Z.; Su, C.; Liu, M.; Shao, Z., A Perovskite Electrocatalyst for Efficient Hydrogen Evolution Reaction. *Adv. Mater.* **2016**, *28*, 6442-6448.
- Wang, J.; Gao, Y.; Chen, D.; Liu, J.; Zhang, Z.; Shao, Z.; Ciucci, F., Water Splitting with an Enhanced Bifunctional Double Perovskite. *ACS Catal.* **2018**, *8*, 364-371.
- 23. Galal, A.; Atta, N. F.; Ali, S. M., Investigation of the Catalytic Activity of LaBO₃ (B=Ni, Co, Fe or Mn) Prepared by the Microwave-Assisted Method for Hydrogen Evolution in Acidic Medium. *Electrochim. Acta* **2011**, *56*, 5722-5730.
- 24. Shan, J.; Ling, T.; Davey, K.; Zheng, Y.; Qiao, S.-Z., Transition-Metal-Doped RuIr Bifunctional Nanocrystals for Overall Water Splitting in Acidic Environments. *Adv. Mater.* **2019**, *31*, 1900510.
- 25. Duan, H.; Li, D.; Tang, Y.; He, Y.; Ji, S.; Wang, R.; Lv, H.; Lopes, P. P.; Paulikas, A. P.; Li, H.; Mao, S. X.; Wang, C.; Markovic, N. M.; Li, J.; Stamenkovic, V. R.; Li, Y., High-Performance Rh₂P Electrocatalyst for Efficient Water Splitting. *J. Am. Chem. Soc.* **2017**, *139*, 5494-5502.
- 26. Wang, W.; Xi, S.; Shao, Y.; Sun, W.; Wang, S.; Gao, J.; Mao, C.; Guo, X.; Li, G., Oxide Passivated CoNi@NC-Supported Ru(OH)_xCl_y Cluster as Highly Efficient Catalysts for the Oxygen and Hydrogen Evolution. *ACS Sustainable Chem. Eng.* **2019**, *7*, 17227-17236.
- 27. Jin, H.; Wang, J.; Su, D.; Wei, Z.; Pang, Z.; Wang, Y., In situ Cobalt—Cobalt Oxide/N-Doped Carbon Hybrids As Superior Bifunctional Electrocatalysts for Hydrogen and Oxygen Evolution. *J. Am. Chem. Soc.* **2015**, *137*, 2688-2694.
- 28. Yue, X.; Zheng, Y.; Chen, Y.; Huang, S., Overall Water Splitting on Ni_{0.19}WO₄ Nanowires as Highly Efficient and Durable Bifunctional non-Precious Metal Electrocatalysts. *Electrochim. Acta* **2020**, *333*, 135554.
- 29. Zhu, Y.; Zhou, W.; Zhong, Y.; Bu, Y.; Chen, X.; Zhong, Q.; Liu, M.; Shao, Z., A Perovskite Nanorod as Bifunctional Electrocatalyst for Overall Water Splitting. *Adv. Energy Mater.* **2017**, *7*, 1602122.
- 30. Larson, A. C.; Von Dreele, R. B., General Structure Analysis System (GSAS), Los Alamos National Laboratory Report LAUR. **2000**, 86–748.
- 31. Toby, B. H., EXPGUI, a Graphical User Interface for GSAS. *J. Appl. Crystallogr.* **2001**, *34*, 210-213.
- 32. Jeerage, K. M.; Candelaria, S. L.; Stavis, S. M., Rapid Synthesis and Correlative Measurements of Electrocatalytic Nickel/Iron Oxide Nanoparticles. *Sci. Rep.* **2018**, *8* (1), 4584.
- 33. Wu, W.; Niu, C.; Wei, C.; Jia, Y.; Li, C.; Xu, Q., Activation of MoS₂ Basal Planes for Hydrogen Evolution by Zinc. *Angew. Chem. Int. Ed.* **2019**, *58*, 2029-2033.

- 34. Zhu, J.; Wang, Z.-C.; Dai, H.; Wang, Q.; Yang, R.; Yu, H.; Liao, M.; Zhang, J.; Chen, W.; Wei, Z.; Li, N.; Du, L.; Shi, D.; Wang, W.; Zhang, L.; Jiang, Y.; Zhang, G., Boundary Activated Hydrogen Evolution Reaction on Monolayer MoS₂. *Nat. Commun.* **2019**, *10*, 1348.
- 35. McGlynn, J. C.; Dankwort, T.; Kienle, L.; Bandeira, N. A. G.; Fraser, J. P.; Gibson, E. K.; Cascallana-Matías, I.; Kamarás, K.; Symes, M. D.; Miras, H. N.; Ganin, A. Y., The Rapid Electrochemical Activation of MoTe₂ for the Hydrogen Evolution Reaction. *Nat. Commun.* **2019**, *10*, 4916.
- 36. Yang, W.; Kim, J. H.; Hutter, O. S.; Phillips, L. J.; Tan, J.; Park, J.; Lee, H.; Major, J. D.; Lee, J. S.; Moon, J., Benchmark Performance of Low-Cost Sb₂Se₃ Photocathodes for Unassisted Solar Overall Water Splitting. *Nat. Commun.* **2020**, *11*, 861.
- 37. Kresse, G.; Furthmüller, J., Efficiency of ab-initio Total Energy Calculations for Metals and Semiconductors Using a Plane-Wave Basis Set. *Comput. Mater. Sci.* **1996,** *6*, 15-50.
- 38. Zunger, A.; Wei, S. H.; Ferreira, L. G.; Bernard, J. E., Special Quasirandom Structures. *Phys. Rev. Lett.* **1990,** *65*, 353-356.
- 39. van de Walle, A.; Tiwary, P.; de Jong, M.; Olmsted, D. L.; Asta, M.; Dick, A.; Shin, D.; Wang, Y.; Chen, L. Q.; Liu, Z. K., Efficient Stochastic Generation of Special Quasirandom Structures. *Calphad* **2013**, *42*, 13-18.
- 40. Trimarchi, G.; Wang, Z.; Zunger, A., Polymorphous Band Structure Model of Gapping in the Antiferromagnetic and Paramagnetic Phases of the Mott Insulators MnO, FeO, CoO, and NiO. *Phys. Rev. B* **2018**, *97*, 035107.
- 41. Hona, R. K.; Huq, A.; Ramezanipour, F., Unraveling the Role of Structural Order in the Transformation of Electrical Conductivity in $Ca_2FeCoO_{6-\delta}$, $CaSrFeCoO_{6-\delta}$, and $Sr_2FeCoO_{6-\delta}$. *Inorg. Chem.* **2017**, *56*, 14494-14505.
- 42. Kim, N. I.; Afzal, R. A.; Choi, S. R.; Lee, S. W.; Ahn, D.; Bhattacharjee, S.; Lee, S. C.; Kim, J. H.; Park, J. Y., Highly Active and Durable Nitrogen Doped-Reduced Graphene Oxide/Double Perovskite Bifunctional Hybrid Catalysts. *J. Mater. Chem. A* **2017**, *5*, 13019-13031.
- 43. Kim, J.; Yin, X.; Tsao, K. C.; Fang, S.; Yang, H., Ca₂Mn₂O₅ as Oxygen-Deficient Perovskite Electrocatalyst for Oxygen Evolution Reaction. *J. Am. Chem. Soc.* **2014**, *136*, 14646-14649.
- 44. Du, J.; Zhang, T.; Cheng, F.; Chu, W.; Wu, Z.; Chen, J., Nonstoichiometric Perovskite CaMnO_{3-δ} for Oxygen Electrocatalysis with High Activity. *Inorg. Chem.* **2014**, *53*, 9106-9114.
- 45. Zhu, J.; Hu, L.; Zhao, P.; Lee, L. Y. S.; Wong, K.-Y., Recent Advances in Electrocatalytic Hydrogen Evolution Using Nanoparticles. *Chem. Rev.* **2020**, *120*, 851-918.
- 46. Šljukić, B.; Vujković, M.; Amaral, L.; Santos, D. M. F.; Rocha, R. P.; Sequeira, C. A. C.; Figueiredo, J. L., Carbon-Supported Mo₂C Electrocatalysts for Hydrogen Evolution Reaction. *J. Mater. Chem. A* **2015**, *3*, 15505-15512.
- 47. Shinagawa, T.; Garcia-Esparza, A. T.; Takanabe, K., Insight on Tafel slopes from a Microkinetic Analysis of Aqueous Electrocatalysis for Energy Conversion. *Sci. Rep.* **2015**, *5*, 13801.
- 48. Hwang, B.-J.; Chen, H.-C.; Mai, F.-D.; Tsai, H.-Y.; Yang, C.-P.; Rick, J.; Liu, Y.-C., Innovative Strategy on Hydrogen Evolution Reaction Utilizing Activated Liquid Water. *Sci. Rep.* **2015**, *5*, 16263.
- 49. Mohammed-Ibrahim, J.; Sun, X., Recent Progress on Earth Abundant Electrocatalysts for Hydrogen Evolution Reaction (HER) in Alkaline Medium to Achieve Efficient Water Splitting A Review. *J. Energy Chem.* **2019**, *34*, 111-160.
- 50. Malkhandi, S.; Trinh, P.; Manohar, A. K.; Jayachandrababu, K. C.; Kindler, A.; Surya Prakash, G. K.; Narayanan, S. R., Electrocatalytic Activity of Transition Metal Oxide-Carbon Composites for Oxygen Reduction in Alkaline Batteries and Fuel Cells. *J. Electrochem. Soc.* **2013**, *160*, 943-952.
- 51. May, K. J.; Carlton, C. E.; Stoerzinger, K. A.; Risch, M.; Suntivich, J.; Lee, Y. L.; Grimaud, A.; Shao Horn, Y., Influence of Oxygen Evolution during Water Oxidation on the Surface of Perovskite Oxide Catalysts. *J. Phys. Chem. Lett.* **2012**, *3*, 3264-3270.
- 52. Jin, C.; Cao, X.; Zhang, L.; Zhang, C.; Yang, R., Preparation and Electrochemical Properties of Urchin-Like La_{0.8}Sr_{0.2}MnO₃ Perovskite Oxide as a Bifunctional Catalyst for Oxygen Reduction and Oxygen Evolution Reaction. *J. Power Sources* **2013**, *241*, 225-230.

- 53. Mohamed, R.; Cheng, X.; Fabbri, E.; Levecque, P.; Kötz, R.; Conrad, O.; Schmidt, T. J., Electrocatalysis of Perovskites: the Influence of Carbon on the Oxygen Evolution Activity. *J. Electrochem. Soc.* **2015**, *162*, 579-586.
- 54. Liang, Y.; Li, Y.; Wang, H.; Zhou, J.; Wang, J.; Regier, T.; Dai, H., Co₃O₄ Nanocrystals on Graphene as a Synergistic Catalyst for Oxygen Reduction Reaction. *Nat. Mater.* **2011**, *10*, 780-786.
- 55. Fabbri, E.; Nachtegaal, M.; Cheng, X.; Schmidt Thomas, J., Superior Bifunctional Electrocatalytic Activity of Ba_{0.5}Sr_{0.5}Co_{0.8}Fe_{0.2}O₃₋₈/Carbon Composite Electrodes: Insight into the Local Electronic Structure. *Adv. Energy Mater.* **2015**, *5*, 1402033.
- 56. Cheng, X.; Fabbri, E.; Nachtegaal, M.; Castelli, I. E.; El Kazzi, M.; Haumont, R.; Marzari, N.; Schmidt, T. J., Oxygen Evolution Reaction on La_{1-x}Sr_xCoO₃ Perovskites: a Combined Experimental and Theoretical Study of their Structural, Electronic, and Electrochemical Properties. *Chem. Mater.* **2015**, *27*, 7662-7672.
- 57. Chen, Y.; Yu, G.; Chen, W.; Liu, Y.; Li, G.-D.; Zhu, P.; Tao, Q.; Li, Q.; Liu, J.; Shen, X.; Li, H.; Huang, X.; Wang, D.; Asefa, T.; Zou, X., Highly Active, Nonprecious Electrocatalyst Comprising Borophene Subunits for the Hydrogen Evolution Reaction. *J. Am. Chem. Soc.* **2017**, *139*, 12370-12373.
- 58. Adolphsen, J. Q.; Sudireddy, B. R.; Gil, V.; Chatzichristodoulou, C., Oxygen Evolution Activity and Chemical Stability of Ni and Fe Based Perovskites in Alkaline Media. *J. Electrochem. Soc.* **2018**, *165*, 827-835.
- 59. Das, D.; Das, A.; Reghunath, M.; Nanda, K. K., Phosphine-Free Avenue to Co₂P Nanoparticle Encapsulated N,P co-Doped CNTs: a Novel non-Enzymatic Glucose Sensor and an Efficient Electrocatalyst for Oxygen Evolution Reaction. *Green Chem.* **2017**, *19*, 1327-1335.
- 60. Xu, X.; Pan, Y.; Zhou, W.; Chen, Y.; Zhang, Z.; Shao, Z., Toward Enhanced Oxygen Evolution on Perovskite Oxides Synthesized from Different Approaches: A Case Study of Ba_{0.5}Sr_{0.5}Co_{0.8}Fe_{0.2}O_{3-δ}. *Electrochim.Acta* **2016**, *219*, 553-559.
- 61. Retuerto, M.; Pascual, L.; Calle-Vallejo, F.; Ferrer, P.; Gianolio, D.; Pereira, A. G.; García, Á.; Torrero, J.; Fernández-Díaz, M. T.; Bencok, P.; Peña, M. A.; Fierro, J. L. G.; Rojas, S., Na-Doped Ruthenium Perovskite Electrocatalysts with Improved Oxygen Evolution Activity and Durability in Acidic Media. *Nat. Commun.* **2019**, *10*, 2041.
- 62. Yao, R.-Q.; Shi, H.; Wan, W.-B.; Wen, Z.; Lang, X.-Y.; Jiang, Q., Flexible Co–Mo–N/Au Electrodes with a Hierarchical Nanoporous Architecture as Highly Efficient Electrocatalysts for Oxygen Evolution Reaction. *Adv. Materi.* **2020**, *32*, 1907214.
- 63. Song, F.; Hu, X., Ultrathin Cobalt–Manganese Layered Double Hydroxide Is an Efficient Oxygen Evolution Catalyst. *J. Am. Chem. Soc.* **2014**, *136*, 16481-16484.
- 64. Jung, S.; McCrory, C. C. L.; Ferrer, I. M.; Peters, J. C.; Jaramillo, T. F., Benchmarking Nanoparticulate Metal Oxide Electrocatalysts for the Alkaline Water Oxidation Reaction. *J. Mater. Chem. A* **2016**, *4*, 3068-3076.
- 65. Lu, B.; Cao, D.; Wang, P.; Wang, G.; Gao, Y., Oxygen Evolution Reaction on Ni-Substituted Co₃O₄ Nanowire Array Electrodes. *Int. J. Hydrogen Energy* **2011**, *36*, 72-78.
- 66. Lee, J. G.; Hwang, J.; Hwang, H. J.; Jeon, O. S.; Jang, J.; Kwon, O.; Lee, Y.; Han, B.; Shul, Y.-G., A New Family of Perovskite Catalysts for Oxygen-Evolution Reaction in Alkaline Media: BaNiO₃ and BaNi_{0.83}O_{2.5}. J. Am. Chem. Soc. **2016**, *138*, 3541-3547.
- 67. Oh, S.; Kim, H.; Kwon, Y.; Kim, M.; Cho, E.; Kwon, H., Porous Co–P Foam as an Efficient Bifunctional Electrocatalyst for Hydrogen And Oxygen Evolution Reactions. *J. Mater. Chem. A* **2016**, *4*, 18272-18277.
- 68. Petrie, J. R.; Cooper, V. R.; Freeland, J. W.; Meyer, T. L.; Zhang, Z.; Lutterman, D. A.; Lee, H. N., Enhanced Bifunctional Oxygen Catalysis in Strained LaNiO₃ Perovskites. *J. Am. Chem.Soc.* **2016**, *138*, 2488-2491.
- 69. Zhang, B.; Lui, Y. H.; Zhou, L.; Tang, X.; Hu, S., An Alkaline Electro-Activated Fe-Ni Phosphide Nanoparticle-Stack Array for High-Performance Oxygen Evolution Under Alkaline and Neutral Conditions. *J. Mater. Chem. A* **2017**, *5*, 13329-13335.

- 70. Pan, Y.; Chen, Y.; Li, X.; Liu, Y.; Liu, C., Nanostructured Nickel Sulfides: Phase Evolution, Characterization and Electrocatalytic Properties for the Hydrogen Evolution Reaction. *RSC Advances* **2015**, *5*, 104740-104749.
- 71. Konkena, B.; junge Puring, K.; Sinev, I.; Piontek, S.; Khavryuchenko, O.; Dürholt, J. P.; Schmid, R.; Tüysüz, H.; Muhler, M.; Schuhmann, W.; Apfel, U.-P., Pentlandite Rocks as Sustainable and Stable Efficient Electrocatalysts for Hydrogen Generation. *Nat. Commun.* **2016**, *7*, 12269.
- 72. Zhu, Y.; Zhou, W.; Sunarso, J.; Zhong, Y.; Shao, Z., Phosphorus-Doped Perovskite Oxide as Highly Efficient Water Oxidation Electrocatalyst in Alkaline Solution. *Adv. funct. mater.* **2016**, *26*, 5862-5872.
- 73. Grimaud, A.; May, K. J.; Carlton, C. E.; Lee, Y. L.; Risch, M.; Hong, W. T.; Zhou, J.; Shao-Horn, Y., Double Perovskites as a Family of Highly Active Catalysts for Oxygen Evolution in Alkaline Solution. *Nat. Commun.* **2013**, *4*, 2439.
- 74. Forslund, R. P.; Hardin, W. G.; Rong, X.; Abakumov, A. M.; Filimonov, D.; Alexander, C. T.; Mefford, J. T.; Iyer, H.; Kolpak, A. M.; Johnston, K. P.; Stevenson, K. J., Exceptional Electrocatalytic Oxygen Evolution via Tunable Charge Transfer Interactions in La_{0.5}Sr_{1.5}Ni_{1-x}Fe_xO_{4±δ} Ruddlesden-Popper Oxides. *Nat. Commun.* **2018**, *9*, 3150.
- 75. Suntivich, J.; Gasteiger, H. A.; Yabuuchi, N.; Nakanishi, H.; Goodenough, J. B.; Shao-Horn, Y., Design Principles for Oxygen-Reduction Activity on Perovskite Oxide Catalysts for Fuel Cells and Metal–Air Batteries. *Nat. Chem.* **2011**, *3*, 546.
- 76. Wang, C.; Zeng, L.; Guo, W.; Gong, C.; Yang, J., Enhancing Oxygen and Hydrogen Evolution Activities of Perovskite Oxide LaCoO₃ via Effective Doping of Platinum. *RSC Adv.* **2019**, *9*, 35646-35654.
- 77. Zhang, Z.; Chen, Y.; Dai, Z.; Tan, S.; Chen, D., Promoting Hydrogen-Evolution Activity and Stability of Perovskite Oxides via Effectively Lattice Doping of Molybdenum. *Electrochim. Acta* **2019**, *312*, 128-136.
- 78. Li, H.; Sun, S.; Xi, S.; Chen, Y.; Wang, T.; Du, Y.; Sherburne, M.; Ager, J. W.; Fisher, A. C.; Xu, Z. J., Metal–Oxygen Hybridization Determined Activity in Spinel-Based Oxygen Evolution Catalysts: A Case Study of ZnFe_{2-x}Cr_xO₄. *Chem. Mater.* **2018**, *30*, 6839-6848.
- 79. Sun, W.; Song, Y.; Gong, X.-Q.; Cao, L.-m.; Yang, J., An Efficiently Tuned d-Orbital Occupation of IrO₂ by Doping with Cu for Enhancing the Oxygen Evolution Reaction Activity. *Chem. Sci.* **2015**, *6*, 4993-4999.

Table of contents

